



Diurnal cycle of water vapor as documented by a dense GPS network in a coastal area during ESCOMPTE-IOP2

Sophie Bastin⁽¹⁾, Cédric Champollion⁽²⁾, Olivier Bock⁽¹⁾,

Philippe Drobinski⁽¹⁾, and Frédéric Masson⁽²⁾

(1) Institut Pierre Simon Laplace/Service d'Aéronomie, Université Pierre et Marie Curie, Paris, France

(2) Laboratoire de Dynamique de la Lithosphère, Université Montpellier II, Montpellier, France

Submitted to the

JOURNAL OF APPLIED METEOROLOGY

Revised manuscript RCK - 517

November 30, 2005

Corresponding author address:

Dr. Sophie Bastin

Earth Observing Laboratory, NCAR

PO Box 3000, Boulder, CO 80307-3000, USA

Tel: 303-497-8760; Fax: 303-497-2044; E-mail: bastind@ucar.edu

ABSTRACT

Global Positioning System (GPS) data from a dense network have been used for the analysis of the diurnal cycle of water vapor over Marseille, France during the second Intensive Observation Period (IOP2, 21-26 June 2001) of the ESCOMPTE field experiment. Both tomographic analyses and integrated water vapor (IWV) contents from GPS have been used, in addition to wind profiler data and surface observations. Tomographic analysis of data from the dense GPS network provided the continuous temporal evolution of the vertical distribution of water vapor over the city of Marseille. The city is located on the shore of the Mediterranean sea in southeastern France and is often under the influence of sea breeze effects. Two different layers of breeze circulation are identified: a shallow sea breeze, blowing perpendicular to the local coastline, and a deep sea breeze induced by the regional temperature gradient between sea and land. The origin of water vapor is shown to be mainly due to the advection of marine moist air by these sea breeze circulations. However, the diurnal cycle of water vapor over Marseille is strongly influenced by the synoptic situation that changes during the IOP2 (between a northerly Mistral in the early stage of the IOP and an easterly wind at the end). It is shown that vertical profiles from tomographic analyses (combined with wind profiler data) allow for a proper interpretation of the diurnal cycle observed in IWV. Two dimensional maps of IWV are also shown to complement the description of the horizontal advection of moisture by the different circulation regimes.

1. Introduction

Marseille is one of the biggest French cities, with about 1 million inhabitants. Facing the Mediterranean sea (Fig. 1), Marseille is frequently under the influence of sea breeze circulations during summertime. These circulations play a key role on the local meteorology (see Simpson, 1994 for a review) and often lead to pollution episodes during anticyclonic situations (e.g Kambezidis et al., 1998; Koo and Reible, 1995). But Marseille is also located in a mountainous area. As a consequence, both terrain heterogeneities and variable topography may induce local atmospheric circulations of various temporal and spatial scales, where maritime and topographic effects interact. In particular, the Mistral is an orographically induced wind that develops along the Rhône valley (Mayençon, 1982; Pettré, 1982; Jiang et al., 2003) and influences the coast of southeastern France and the western Mediterranean climate. It is frequently observed to extend as far as a few hundreds of kilometers from the coast (Jànsa, 1987). But sometimes, the weakness of the Mistral allows the sea breeze to break through along the coast (Bastin et al., 2006; Guénard et al., 2005). The complex interaction between land/sea breezes, slope winds and larger scale winds as the Mistral significantly affects the three-dimensional (3D) water vapor distribution and its variability and the local dynamics of convection.

The ESCOMPTE experiment (ExperimentS to CONstrain Models of atmospheric Pollution and Transport of Emissions) took place in the region of Marseille during summer 2001 (Cros et al., 2004). The instrumental set-up allowed to document the dynamics and chemistry over the region. In particular, it was well suited to observe and investigate several

Mistral cases, sea breeze cases and also the dynamics of the interaction between the sea breeze and the Mistral (Bastin et al., 2006). Moreover, during this experiment, a dense GPS (Global Positioning System) network was deployed in the region for the study of the variability of atmospheric water vapor (Bock et al., 2004). This network gives access to two types of products. The first one is Integrated Water Vapor (IWV). It is usually used to analyze the temporal variability of total column humidity at each station. Horizontal maps can be constructed from spatial interpolation of IWV between stations. However, the IWV content does not indicate where the water vapor is located in the atmospheric column. GPS tomography allows for retrieval of both the vertical and horizontal distribution, as well as the temporal evolution of water vapor in the lower troposphere. It is a recent technique that requires GPS observations from a dense network. The network deployed during the ESCOMPTE campaign was specifically designed to allow for tomographic analysis.

The goal of the paper is to study how the synoptic situation influences the diurnal cycle of the migration of moisture over Marseille. The GPS network and its derived products IWV and tomography make this study possible and it will help in the scientific understanding of the water vapor transport in this region, which is not well known due to the lack of water vapor observations. This study is limited to a 6-day period, corresponding to the second Intensive Observing Period (IOP) of the experiment, which covered two different synoptic situations. The first is an alternation of sea breeze and Mistral wind, and the second is an alternation of sea breeze / land breeze.

Section 2 presents the instrumental set-up and the different products obtained from the GPS network, while section 3 presents the meteorological situation. The analysis of the

diurnal cycle of water vapor as a function of the synoptic situation is described in section 4. Section 5 concludes this study.

2. Measurements and data analysis

a. Instrumental set-up

During summer 2001, meteorological measurements were taken in southern France (see Fig. 1) in the framework of the ESCOMPTE experiment (Cros et al., 2004). In the present study, we use the measurements from a meteorological surface stations network, radiosondes, a UHF radar and a GPS network (Bock et al., 2004) located within the city of Marseille (Fig. 1c).

Radiosondes were launched from Aix-les-Milles (see AIX in Fig. 1b), located 25 km to the north of Marseille, several times a day. On some rare days, some radiosondes were also launched from the center of Marseille.

The UHF wind profiler was located in the center of the city of Marseille, close to the GPS station named CINQ (Fig. 1c). The measurements consist of the time evolution of the vertical profiles of the three wind components thanks to one vertical beam and two oblique beams, slanted at an off-zenith angle of 17° , the half-power beamwidth being 8.5° . The radar works with a frequency of 1238 MHz and with a peak power of 4 kW. The wind velocity is estimated from the frequency corresponding to the mean Doppler shift obtained in the radar echo. The data quality control and processing are carried out through a consensus algorithm based on time and height continuity of measured spectra. The consensus works

over a 60-min period providing a wind profile each 15-min from a height of 100-300 m up to 2500-4000 m above ground level (AGL). The vertical resolution is typically 75-150 m. The errors on the horizontal wind measurements are 1-2 m s⁻¹.

The GPS network consisted of 17 GPS receivers with a mean distance between them of about 5 km (see the box in Fig. 1b). The network was designed to provide data for the validation of a tomographic analysis model developed at Laboratoire de Dynamique de la Lithosphère (Champollion et al., 2005). GPS tomography also proved to be ideally appropriate for validation of fine-scale numerical simulations of water vapor fields (Bastin et al., 2005). For the present study, tomographic fields are retrieved with a 30 min interval, a horizontal grid mesh of 0.05° and a vertical cell size ranging from 500 m near the ground to 1000 m at 10 km altitude.

b. GPS water vapor retrieval

The basic GPS atmospheric product is the tropospheric delay. This quantity is a measure of delay of the GPS signal that has travelled between a GPS satellite (at 20200 km altitude) and a ground based receiver with respect to propagation in a vacuum. The standard procedure for GPS data analysis assumes that the delay in any direction can be mapped from the delay at zenith to which a horizontal gradient is added. Three sets of parameters are then estimated during the analysis: zenith tropospheric delays (ZTDs), gradients and post-fit residuals which are the difference between the modelled atmosphere and the measurements. From the ZTD, the component due to the dry atmosphere is removed and the remainder is converted into IWV. ZTD is thus mapped into IWV, using simply surface pressure and

temperature and empirical formulae (Davis et al., 1985; Bevis et al., 1992; Emardson and Derks, 1999). The accuracy in GPS IWV has been assessed by a number of authors, using intercomparisons with radiosondes, microwave radiometers, sun photometers, lidars and Very Long Baseline Interferometry (Foelsche and Kirchengast, 2001; Niell et al., 2001; Bock et al., 2004). The agreement between these techniques is about 1-2 kg m⁻².

For the tomographic analysis of tropospheric water vapor, slant integrated water vapor (SIWV) contents are required. These contents are retrieved from a post-processing of GPS ZTD, gradient and residuals estimates. First, slant delays are reconstructed by mapping ZTD and gradients into the direction of the GPS satellites. Then, the dry atmosphere is removed. The procedure is the same as for IWV but an estimate of the dry gradient is required. Therefore, 2D surface pressure measurements are used, following Elòsegui et al. (1999). Finally, the post-fit residuals are added corrected by using stacking maps (Shoji et al., 2004).

The tomographic analysis consists of retrieving the scalar three-dimensional field of water vapor density from the integrated quantities. Since we consider the geometrical effect of the bending of the ray as negligible for elevation angles higher than 10° (Elgered, 1993), the problem becomes linear. The formulation in the linear discrete theory of the direct problem expresses the link between the observations (SIWV) Y and the true water vapor density X (expressed in g m⁻³) through the linear operator \mathbf{M} :

$$Y = \mathbf{M}X + \varepsilon \quad (1)$$

where ε is the measurement error vector. The linear operator \mathbf{M} is expressed as a matrix

whose coefficients represent the length of each ray in each cell.

To solve the inverse problem, the matrix \mathbf{M} must be inverted. As the problem is locally underdetermined, we have to find the "generalised inverse" \mathbf{M}^{-g} to obtain the reconstructed field X_{reco} from the data Y :

$$X_{reco} = \mathbf{M}^{-g}Y \quad (2)$$

To minimize the ill-conditioning, some constraints can be added using external water vapor measurements such as humidity profiles from radiosoundings as shown in the following. More details about processing procedure for the ESCOMPTE GPS data can be found in Walpersdorf et al. (2004) and Champollion et al. (2005). The latter reference also presents a validation of tomographic retrievals from ESCOMPTE data.

The GPS tomography without vertically resolved data assimilated allows to retrieve the 3D field of water vapor density with limitation on the vertical resolution due to geometrical configuration of the GPS network. Indeed, if the lateral variations of density can be resolved, several studies have shown that some structures could never been imaged whatever the number of GPS stations of the network (Leveque and Masson, 1999; Champollion et al., 2005). Several different vertical distributions of water vapor density above the highest GPS station could fit the tomographic inversion. Nevertheless, the GPS tomography provides a realistic (which may be different from the truth) vertical distribution of water vapor density which is not constant and equal to the height of the tomographic grid divided by the IWV value for example. The topography is indeed contributing to a good resolution but only in the first levels (Flores et al., 2000; Champollion et al., 2005). However, given a realistic a priori

model, the tomography reproduces the water vapor fields that satisfy the condition that as much moisture is mapped to the lower levels above the highest GPS station as is possible given the observations. Thus, the model represents the minimum boundary layer height that is possible. The tomography shows a *possible* model that fits the data. The assimilation of vertically resolved data such as radiosondes or lidar profiles is therefore necessary to discuss the real variations of water vapor above 1 km AGL.

The tomography is done with the software *LOFTT_K* developed in the Laboratoire Dynamique de la Lithosphere (Champollion et al., 2005). Some improvements have been done since. First, to follow the time variations of the water vapor a Kalman filtering has been implemented. Secondly, the software allows the assimilation of water vapor profiles from various instruments. The potentiality has been used only with the radiosondes data to constrain the vertical distribution of water vapor. Other data such as radio occultation, lidar or radiometer profiles could be assimilated in the same way.

The Kalman filter is only used as an assimilation tool, the model for the temporal transition between two consecutive times is an identity matrix without any physical equations. The initialization of the filter is done by an interpolation of the radiosondes available at the closest released time. The initialization of the model error is done following Gradinarsky (2002) with an exponential law and a characteristic height scale of 3 km. The correlation of the errors of the initial model is modelled as a Gaussian function with a characteristic scale of 25 km in horizontal and 500 m in vertical to reflect the high vertical variability of the water vapor density. The choice of the initial model is not critical and the start time of the filter is closed to a radiosonde launch.

At each correction step all the available GPS and the radiosonde data are assimilated to correct the previous model. The measurement error covariance can be split into two different parts: the discretization and the observation (ZTD GPS estimate and errors in the conversion to SIWV). The discretization error (based on direct modelling of real data into different grids) shows a white noise level of 2 for $0.05^\circ \times 0.05^\circ \times 500$ m cells, with no bias and no correlation. The ZTD error (typically 6 mm) is projected to the direction of the ray path. The error of the GPS data and the conversion from delay to integrated water vapor density is a compilation of all the errors from the previous references about the GPS data processing projected from the zenith to the elevation angle of the slant with the Niell mapping function. The correlations of the GPS slant errors are assumed only on the zenith measurements (not in the gradient, not in the residuals) depending on the time separation between the two slants and the distance between the two GPS sites. Following the rare studies about GPS errors correlation (Jarlemark et al., 2001; Haase et al., 2003), we chose 50 km for the horizontal exponential correlation scale and 60 mn for the time scale. The radiosoundings errors are assumed uncorrelated. The radiosoundings dataset for the six days of the study is composed of 19 radiosoundings. 16 of them are located in Aix-les-Milles, 25 km to the north of Marseille, and 3 are located near the GPS station CINQ in the centre of the GPS network. The error is the sum of the measurement errors and a factor of 10 corresponding to the expected variability of the water vapor field within the tomographic cell. A radiosounding influences a cell with a Gaussian law function of the distance between the centre of the cell and the position of the radiosounding and of difference of time between the radiosounding and its assimilation. The characteristic scales are 50 km and 1 hour for

distance and time. The grid follows the terrain topography to avoid variation of the depth of the first level. The Kalman filter is updating every 30 minutes. As the GPS SIWV are evaluated every 5 minutes with about 8 satellites in view for each of the 18 GPS stations, about 900 integrated water vapor slants rays are assimilated every 30 minutes.

At each prediction step, the model error is increased to allow the variation of the model within time. The increase of the error model is dynamically controlled by the error between the predicted model and the measurements: the more the predicted model is away from measurements, the more the background error is dilated. The technique allows to adapt dynamically the filter to the slow or rapid variations of the real 3D field of water vapor.

The assimilation scheme seems to be working sufficiently well (with enough degree of liberty) for the GPS data to influence the radiosounding data without discontinuity. The tomography fits well with the data in place and time of the radiosoundings launch. During the 6 days of the POI2, we have compared the radiosoundings and the tomographic results. With or without assimilation, no bias is found. The dispersion is equal to about 1 g m^{-3} without assimilation and better than 0.5 g m^{-3} with the assimilation scheme. The residual dispersion between the tomography with the radiosounding assimilated is due to errors in the SIWV and the water vapor variability for the radiosounding from Aix-les-Milles (25 km to the north of the GPS network).

3. The Intensive Observing Period IOP2: 21-26 June 2001

During IOP2, two types of situations were encountered. The first three days of the IOP2 (hereafter called IOP2a), i.e. 21, 22 and 23 June 2001, the Mistral dominated. The Mistral

is a dry northwesterly flow channeled within the Rhône valley (Fig. 1). During IOP2a, it blows at night within a 2 km-deep layer and is lifted up during the day as the southwesterly sea breeze penetrates inland beneath the Mistral flow (Bastin et al., 2006; Guénard et al., 2005). During the last three days of the IOP2 (hereafter called IOP2b), i.e. 24, 25 and 26 June 2001, northeasterly land breeze at night alternates with sea breeze flow during the day.

a. IOP2a (21-23 June 2001): interaction of sea breeze with the Mistral

Figure 2a and b presents the synoptic charts on June 22 at 0000 UTC (a) and 1200 UTC (b). Note that the synoptic situation of the other days of the IOP2a is similar to that of June 22, so only the latter one is presented here. The IOP2a Mistral event is featured by a northwesterly flow over France resulting from an anticyclone over western France and a low-pressure system over northern Europe. On June 22 at 0000 UTC (Fig. 2a), a high surface pressure zone (1020 hPa) is located north and west from Ireland and extends over France, contributing to very weak surface winds upstream the Massif Central and the Alps. In southeastern France, a cyclone is visible in the Gulf of Genoa which is a classic Mistral situation. However it remains weak with respect to other Mistral events (see for instance Guénard et al., 2005 and Drobinski et al., 2005). It extends from the Pyrénées to the Pô valley (see Fig. 1). On June 22 at 1200 UTC (Fig. 2b), the Genoa cyclone is removed but the curvature of the isobars is still important, associated to surface pressure gradient which is favorable to large cyclonic curvature of the Mistral at the exit of the Rhône valley. Figure 3a and b displays the wind and temperature fields from meteorological surface stations on June 22 at 0000 UTC (a) and 1200 UTC (b). It clearly shows the intensification of the northerly

flow in the Rhône valley and the sheltered area from the Mistral in the wake of the Alps (eastern side of the considered area). Note that at 1200 UTC, no sign of sea breeze is visible in the Rhône valley delta.

b. IOP2b (24-26 June 2001): alternation of sea breeze and land breeze

Figure 2c, d, e and f presents the synoptic charts on June 25 (c and d) and June 26 (e and f) at 0000 UTC (left panels) and 1200 UTC (right panels). The situation on June 24 is similar to those on June 25 and is not presented here. At the beginning of this period, a ridge extends from Morocco to Norway. It generates a north-westerly synoptic wind in altitude over southern France. On June 25, the surface pressure is high, inducing anticyclonic conditions. At 850 hPa (not shown), the pattern indicates no significant pressure gradient over France and the Mediterranean sea. These conditions are propitious to the development of a sea-breeze circulation. Figure 3 c and d displays the wind and temperature fields from meteorological surface stations on June 25 at 0000 UTC (c) and 1200 UTC (d). Fig. 3c shows no significant surface temperature gradient. At 1200 UTC (Fig. 3d), a temperature gradient appears near the coastline that drives the sea breeze flow.

On June 26, the ridge at 500 hPa level stays over France but the surface high pressure moves eastward. Consequently, the synoptic flow weakens and veers from the northwest on June 25 to the west on June 26. At 1200 UTC (Fig 2f), a surface low pressure is located over southern Ireland generating southerly low-level winds over France. Figure 3f clearly shows the combination between the sea breeze flow generated by the temperature gradient near the coastline and the southerly synoptic flow. Based on the above observations, a pollution

episode was predicted to occur during IOP2b (24 to 26 June 2001).

c. Vertical structure of the air flow over Marseille

Figures 4a and b display vertical profiles of wind speed (panel a) and wind direction (panel b) as a function of time from UHF measurements over Marseille between June 21 and June 26. The UHF was located in the center of the city, near the GPS station named CINQ (see Fig. 1c). This figure clearly shows the differences and the transition between IOP2a and IOP2b.

During IOP2a, the diurnal cycle is well marked. Between 0000 and 1200 UTC, the wind direction is north-northwesterly from the ground up to 2 or 3 km. In this layer, the wind speed ranges from 3 to 5 m s⁻¹ near the ground and can reach 20 m s⁻¹ at 1 km height and above. This provides evidence that the whole layer between the surface and 3 km is affected by the presence of the Mistral, whose intensity is weaker near the surface due to friction. During the afternoon, two different layers are apparent. In the first layer, i.e from the surface up to about 600 m AGL, the wind direction is westerly-southwesterly, associated with wind speeds of about 5-8 m s⁻¹, while in the second layer, i.e from 600 m up to 2-3 km, the wind direction is again north-northwesterly, associated with an intensity of 7-12 m s⁻¹. The existence of these two layers indicates the onset of the sea breeze in the afternoon (i.e at about 1100 UTC on June 21, at about 1500 UTC on June 22 and at about 1300 UTC on June 23) near the coastline that lifts the Mistral up to 700 or 800 m. The weakness of the Mistral during this period allows the sea breeze to break through near the coastline where the temperature gradient between land and sea is maximum. Thus, during IOP2a,

the Mistral that blows near the surface during nighttime is not strong enough to inhibit the sea breeze (Arritt, 1993) and is replaced by a sea breeze flow near the surface during the afternoon.

The transition between IOP2a and IOP2b occurs during the afternoon of June 23, where the Mistral weakens due to the dissipation of the Genoa cyclone near the surface. During IOP2b, the diurnal cycle is not as well marked as during IOP2a. The wind speed is nearly the same during nighttime and daytime, even though we can distinguish a light intensification of the wind during the afternoon, and it is rather homogeneous with height. It ranges from 1 to 5 m s⁻¹ from the ground up to 2 km. However, the wind direction shows the existence of a diurnal cycle especially near the surface where the wind alternates from westerly during daytime to easterly during nighttime. Here we can distinguish several layers. Between the surface and about 300-400 m AGL, the wind blows perpendicular to the shoreline (see Fig. 1 for the coastline shape), i.e from the west during the day (sea breeze) and from the east during night (land breeze). This direction near the surface is due to the local sea breeze which follows the local maximum temperature gradient direction. This sea breeze is called the "shallow sea breeze" (SSB) (Banta, 1995; Bastin and Drobinski, 2006; Lemonsu et al., 2006). It starts blowing at about 1000 UTC on June 24 and June 25, and at about 1200 UTC on June 26. Above, from about 400 m AGL up to 1300 m, the wind direction is not the same during the whole IOP2b. On June 24, the synoptic situation induces a north-westerly flow in this second layer. On June 25, during the day, the wind has a southerly direction corresponding to the direction of the mesoscale temperature gradient that drives the "deep sea breeze" (DSB) which blows above the SSB (Bastin and Drobinski, 2006; Lemonsu et al.,

2006). During the night and in the morning, this DSB does not exist and a westerly flow blows. On June 26, the synoptic wind blows from the east. It has been shown that, on June 26, the low level air mass, up to 2 km AGL, skirts the Mediterranean coast over land from the east-south-east (Lemonsu et al., 2006).

4. Water vapor diurnal cycle over Marseille

a. Vertically resolved water vapor

Figure 4c shows vertical profiles of water vapor density versus time from GPS tomography over Marseille, at 5.375°E longitude and 43.325°N latitude. The vertical distribution and diurnal variation of water vapor are clearly different between IOP2a and IOP2b. A strong diurnal modulation is observed during IOP2a while this modulation has a smaller amplitude and is limited to a shallower layer during IOP2b. During IOP2a, a strong vertical gradient of water vapor exists in the first 3 km with values ranging from 9-10 g m⁻³ for the maximum (light blue) to 0-2 g m⁻³ (red colors) at an altitude inferior to 3 km. The thickness of this layer where all the water vapor is concentrated (all colors except red) has a marked diurnal cycle. It ranges from 1.7-2.0 km in the late night and morning to 3.0 km in the afternoon. The maximum values of water vapor density near the surface show the same diurnal variation, with a maximum of about 9-10 g m⁻³ in the afternoon and a minimum of about 4 g m⁻³ in the late morning. During IOP2b, two different layers that both contain water vapor are apparent. The lower layer (blue, green and yellow colors) is not homogeneous with height. The values ranges from 12-13 g m⁻³ near the surface down to 6-7 g m⁻³ at about 1.5-2.0 km.

This layer is located below a drier and more homogeneous layer of 2 to 4 g m⁻³ (light brown and orange colors), which tops at more than 3.5 km (not shown), except on June 26 in the presence of an easterly wind regime.

During IOP2a, the dry northwesterly Mistral, which blows up to 2-3 km AGL, leads to a much drier free troposphere over Marseille than during IOP2b. The onset of the sea breeze is quite late, around 1500 UTC on June 22, which limits the daytime accumulation of humidity. The maximum of water vapor is reached at about 1800 UTC, which is consistent with surface station measurement in the northern suburbs of Marseille (see Bastin et al., 2005). The vertical extension of the 'moist' layer (all colors except red) is likely to be induced by the enhanced turbulent mixing, resulting from the detrainment of water vapor from the sea breeze flow onto the free troposphere aloft (Bastin and Drobinski, 2006). At night, the dry Mistral flow reaches the ground and blows within a 2 km-depth layer, hence exporting most of the water vapor accumulated during daytime. The contrast in total water vapor content and vertical distribution is thus marked between night and day.

During IOP2b, the maximum of water vapor (dark blue color) is reached late in the evening (later than 22 UTC on June 23, June 24 and June 26, earlier on June 25). At night, weak land breeze circulation blows over Marseille which partly exports the moist air imported during the day by the sea breeze. The effects of the land breeze are thus not immediate due to its weak intensity. However, the contrast in stratification and total column content of water vapor between day and night is very small. This small contrast during days June 23 (from midday), June 24 and June 25 is due to: (i) local radiative cooling and condensation which reduce the amount of water vapor during night (in contrast with the Mistral which

advected continental dry air masses on synoptic scale during IOP2a); (ii) the weakness of the land breeze near the surface (at most 2 m s^{-1}) and of the synoptic flow above (at most 5 m s^{-1}), which are not as efficient as the Mistral in exporting the air mass that accumulated moisture during daytime. As a consequence, total column humidity is nearly constant, and in fact slightly increases between June 24 and June 25. During the night between June 25 and June 26, the dry easterly flow acts as the Mistral during nighttime of IOP2a.

b. Vertically integrated water vapor

Total column humidity, or IWV, is the common atmospheric GPS product which can be retrieved from single stations. It quantifies the amount of water vapor available in the column of atmosphere. This variable is related to the quantity of rain that may fall if convection occurs, though the relationship between IWV and precipitation is not obvious. IWV is generally not easy to interpret alone, and requires the combined analysis with surface and upper air thermodynamic variables. In the present case study, IWV time series can be interpreted with the help of wind profiler (Fig. 4a and b) and vertical moisture distribution from tomography (Fig. 4c). This section thus provides a description and interpretation of IWV using the vertically resolved observations presented in the previous sections.

Figure 4d shows the time series of the IWV from the GPS measurements at CINQ, in the center of Marseille, and VALL, 6 km to the north of the former (Fig. 1c). We first analyse the time series at CINQ. In these time series, the two periods of interest are clearly distinct: (1) the mean IWV over IOP2a is 15.5 kg m^{-2} , while it amounts to 21.7 kg m^{-2} during IOP2b; (2) the amplitude of the diurnal variations about the mean IWV are much

larger during IOP2a (5, 9, and 12 kg m⁻² for June 21 to June 23) than during IOP2b (3.5, 5.5, and 5 kg m⁻² for June 24 to June 26). The two special cases of June 23, marked by the dissipation of the Mistral, and June 26, marked by an easterly wind regime, are discernible.

The lower IWV mean value and the greater amplitude of variations around the mean value during IOP2a are explained by: (i) the drier free troposphere over Marseille, (ii) the smaller vertical extent of the sea breeze, (iii) the later onset of the sea breeze (around 15 UTC) and peaking of humidity in the boundary layer (around 1800 UTC), which limits the daytime accumulation of humidity, and (iv) the transport of humidity offshore during nighttime by the Mistral flow which reaches the ground and blows within a 2 km-depth layer.

During the night from June 25 to June 26, the large decrease of the IWV mean value is mainly due to the large-scale drier continental air blowing from the east. During the daytime of June 26, this flow veers to the south-east and combines with the sea breeze flow, hence increasing IWV again by the end of the day. During daytime, the impact of the synoptic-scale flow is quite different from IOP2a where the Mistral flow blows in nearly the opposite direction to the sea breeze flow. Also, the maximum IWV is reached late in the evening because this synoptic-scale (south-easterly) flow does not reverse and consequently inhibits the creation of a land breeze (Arritt, 1993).

By comparing IWV observed at VALL and CINQ (Fig. 4d), interesting differences are apparent. Actually, CINQ has more IWV throughout the time series but the differences are larger during IOP2b. The differences of IWV are mainly due to the location of the two stations: CINQ station is in the center of the city of Marseille, at an altitude of 131 m above sea level (ASL), while VALL is located in the northern suburbs of Marseille, further

to the coastline, at an altitude of 314 m ASL. The differences of altitude and distance from the coastline create the lower level of IWV at VALL during the whole IOP2. The complex sea breeze circulation over Marseille induces the stronger differences of IWV during IOP2b. Indeed, during sea breeze regime, the SSB has mostly a westerly direction at VALL (see the coastline shape in Fig. 1), while CINQ is in the convergence zone between the two SSBs: the westerly SSB that enters Marseille by its western coast and the southerly SSB that enters Marseille by its southern coast. Consequently, more moist air reaches CINQ and IWV values are higher than observed at VALL. Moreover, the massif de l'Etoile, culminating at 600 m ASL to the north of Marseille, might induce some flow blocking and thus accumulation of water vapor in the center of the city. This is especially observed during IOP2b, when the diurnal cycle is controlled by the alternation of land and sea breezes.

c. Horizontal variability

As discussed above, the temporal evolution of the vertical distribution of water vapor and IWV is strongly linked to horizontal flow in different layers: from the local SSB to the regional DSB and synoptic scale circulation. With the data at hand, the horizontal distribution of water vapor can be analysed from either horizontal cross-sections of water vapor density obtained from the tomographic analyses (as used in Bastin et al., 2005) or from two-dimensional (2D) maps of IWV. Though the GPS network operated during ESCOMPTE covers a very small area, significant differences in IWV are observed between stations. We therefore used IWV maps to analyse the evolution of the 2D horizontal distribution of IWV during June 22, June 25, and June 26. These maps confirm and complement the analysis

from the previous sections.

Figure ?? shows that there is a persistent north-south gradient in IWV, due to the local topography (as discussed above). Panels a, b, and c show the evolution for June 22. This is a typical case of sea breeze development under a moderate Mistral. At 0600 UTC, the average IWV is quite low (about 10 kg m^{-2}), with a quite uniform IWV content over the central part of the domain. During this period, the Mistral advects dry and cold continental air over the whole domain. At 1200 UTC, the atmospheric boundary layer starts to deepen and moisten, and the Mistral flow layer raises due to convective eddies in the convective boundary layer. However, no clear gradient is seen because of the late establishment of the sea breeze over Marseille. Actually, the synoptic Mistral flow inhibits the sea breeze flow until 1500 UTC. Finally, during the afternoon, the sea breeze becomes strong enough to lift the Mistral up to 700 or 800 m (Fig. 4a and b). The air becomes then significantly more humid. At 1800 UTC, the IWV content reaches 20 kg m^{-2} over the southern part of the domain and there is a marked north-south, as well as a smaller east-west, gradient. This gradient is a result of the combination of a southerly and westerly inflow, since the SSB blows perpendicular to the local direction of the coastline (see section 3. c).

Figure ??d, e, and f provide a similar view for June 25, which is a typical case of a daily sea breeze development following a nocturnal land breeze. The average IWV is much higher than in the previous case (about 25 kg m^{-2} at 0600 UTC). At 0600 UTC, there is a strong north-south gradient throughout the domain, which follows the land breeze flow exporting moisture to the sea (mainly to the south). However, as already mentioned, the land breeze is not as efficient as the Mistral to dry up the atmosphere (and hence the quite large IWV

observed at 0600 UTC, about 22-25 kg m⁻² in the center of the domain). On June 25, the sea breeze onset occurs earlier (shortly after sunrise) in the morning than during IOP2a. At 1200 UTC, the SSB blows again from south and west, and IWV is increasing to 30 kg m⁻² in the central area. At 1800 UTC, the humidity starts to decrease in the western part of the city, in agreement with Fig. 4d where the maximum of humidity is observed around 1600 UTC.

Figure ??g, h, and i show a very different IWV pattern and evolution for June 26. After an overall drop in IWV during the night, the synoptic flow is from east to south-east during most of the day, which combines with the south-westerly sea breeze. At 0600 UTC, the average IWV is about 18 kg m⁻², and the gradient is oriented toward the south-east. The average IWV goes on decreasing after 0600 UTC until 15 kg m⁻². At 1200 UTC, the gradient is more easterly to the south of the domain, in response to the easterly synoptic flow, and IWV has mostly increased in the eastern part of the domain. Indeed, Lemonsu et al. (2006) show that the air mass that reaches Marseille from the east, initially comes from the south over the Mediterranean sea and it then brings some humidity. Fig. ??h shows that IWV has also increased in the western part of the domain, where the westerly SSB enters the city of Marseille. At 1800 UTC, both the easterly-southeasterly gradient and the peak over the city center are reinforced due to the persistence of moisture accumulation from both flows.

5. Conclusion and perspectives

The first conclusion from this study is that the water vapor variability, even observed in a small domain (20 km x 20 km in our case), has a multiscale nature. Indeed, the water

vapor above Marseille has a local origin since it is mainly advected by the shallow sea breeze that blows near the surface and perpendicular to the coastline shape. However, the large scale synoptic flow has a strong impact on the content of moisture in the lower troposphere. It can modify the development of the sea breeze flow (depth, onset time, inland penetration) and its diurnal cycle. It has been shown that the synoptic-scale dry continental Mistral wind is very effective at exporting moisture offshore at night that was enhanced by the daily sea breeze flow. Similarly, a synoptic scale flow can also enhance the daily sea breeze and lead to the accumulation of moisture inland. Such a situation was encountered at the end of IOP2 with a south-easterly flow.

The GPS data from the ESCOMPTE experiment proved to be valuable for the description of the 4D water vapor variability at small scales. This description was relevant for the analysis of the diurnal cycle of water vapor over the city of Marseille, France. However, GPS data alone are generally not sufficient for a proper comprehension of the atmospheric processes acting in such a case study. The combination of vertical profiles of humidity from GPS tomography with wind profiler data was necessary for understanding the diurnal cycle of water vapor in a typical atmospheric column (in the center of Marseille). The diurnal cycle of IWV from GPS data could then be interpreted properly in the context of the local circulation and the vertical distribution of water vapor density. A comparison between two GPS stations showed that slight differences in the diurnal cycle of IWV can be observed even from nearby stations (6-km apart). This difference could be related to the local topography. It became evident from 2D maps of IWV that a persistent gradient in IWV followed the topography. Gradients in IWV were also related to the direction of the

flow in the lower troposphere. The temporal evolution observed in 2D maps also provided important information on the origin of the humid air masses advected from the sea breeze or synoptic scale flows.

A second important conclusion is that the different GPS products available from the present experimental data each provided a complementary view of tropospheric water vapor variability. From a methodological point of view it was important to show that much information is contained in the IWV times series and that it can be interpreted in combination with a few other observational data but that neither model simulations nor assimilation of the GPS data are mandatory for such a study.

In this study, the rapid evolution of the vertical distribution of water vapor was provided from GPS tomography, with a 30 minutes/500 m resolution. Only few other observational techniques can provide such data. One of the main advantages of the GPS technique is its all weather capability, hence providing a continuous monitoring of the atmosphere. However, the vertical resolution in the tomographic analysis is linked to the density of the GPS network. In the case of the ESCOMPTE experiment, a well designed network was deployed. The question to be addressed next is the capability of the GPS tomography technique over larger and sparser networks, such as permanent networks. Such a test is currently under investigation with data from the International H₂O Project, IHOP, (Weckwerth et al., 2004). Another way to exploit water vapor observations from GPS data is to assimilate them in atmospheric models. Significant benefit could be achieved with GPS data if slant delays or SIWV contents would be assimilated, as they provide information on the anisotropy of the water vapor field not contained in IWV (Falvey and Beavan, 2002; MacDonald et al., 2002).

Acknowledgments. The authors would like to thank A. Walpersdorf for contributing to the analysis of the GPS data. The authors are also very grateful to T. Weckwerth and the reviewers for their relevant comments and their help in improving the paper. They are thankful to B. Cros and P. Durand for the coordination of the ESCOMPTE experiment; E. Doerflinger for the coordination of the GPS experiment. They also acknowledge the Institut National des Sciences de l'Univers (INSU) of the Centre National de la Recherche Scientifique (CNRS) through the Programme National de Télédétection Spatiale (PNTS) and the Institut Géographique National (IGN) who supported the GPS field experiment. The ESCOMPTE steering committee and the major French contributors to the ESCOMPTE field campaign [Agence De l'Environnement et de la Maîtrise de l'Énergie (ADEME), Ministère de l'Aménagement du Territoire et de l'Environnement (MATE), INSU, and Météo-France] are also acknowledged. The authors would also like to acknowledge the people from Marseille who kindly accepted to host a GPS receiver in their gardens or on the roofs of their houses.

References

- Arritt, R.W., 1993: Effects of the large scale flow on characteristics features of the sea breeze. *J. Appl. Meteor.*, **32**, 116-125.
- Banta, R.M., 1995: Sea breezes shallow and deep on the california coast. *Mon. Wea. Rev.*, **123**, 3614-3622.
- Bastin, S., C. Champollion, O. Bock, P. Drobinski, and F. Masson, 2005: On the use of GPS tomography to investigate water vapor variability during a Mistral/sea breeze event in south-eastern France. *Geophys. Res. Let.*, **32**, No5, L05808.
- Bastin, S., P. Drobinski, V. Guénard, J.L. Caccia, B. Campistron, A.M. Dabas, P. Delville, O. Reitebuch, and C. Werner, 2006: On the interaction between the sea breeze and a summer Mistral event at the exit of the Rhône valley. *Mon. Wea. Rev.*, in press.
- Bastin, S., and P. Drobinski, 2006: Sea breeze induced mass transport over complex terrain in southeastern France: A case study. *Quart. J. Roy. Meteorol. Soc.*, in press.
- Bevis, M., S. Businger, T. Herring, C. Rocken, R.A. Anthes, and R.H. Ware, 1992: GPS meteorology: remote sensing of the atmospheric water vapor using the Global Positioning System. *J. Geophys. Res.*, **97**, 15787-15801.
- Bock, O., E. Doerflinger, F. Masson, A. Walpersdorf, J. Van-Baelen, J. Tarniewicz, M. Troller, A. Somieski, A. Geiger, and B. Bürki, 2004: GPS water vapor tomography project: Description and first results of the ESCOMPTE field experiment. *Phys. Chem. Earth*, **29**, 149-157.
- Champollion, C., F. Masson, M.N. Bouin, A. Walpersdorf, E. Doerflinger, O. Bock, and J. Van

Baelen, 2005: GPS Water vapour tomography: Preliminary results from the ESCOMPTE field experiment. *Atmos. Res.*, **74**, 253274.

Cros, B., P. Durand, H. Cachier, P. Drobinski, E. Fréjafon, C. Kottmeier, P.E. Perros, V.-H. Peuch, J.-L. Ponche, D. Robin, F. Saïd, G. Toupance, and H. Wortham, 2004: The ESCOMPTE program. An overview. *Atmos. Res.*, **69**, 241-279.

Davis, J.L., T.H. Herring, I.I. Shapiro, A.E.E. Rogers, and G. Elgered, 1985: Geodesy by radio interferometry: Effects of atmospheric modeling errors on estimation of baseline length. *Radio Sci.*, **20**, 1593-1607.

Drobinski, P., S. Bastin, V. Guénard, J.-L. Caccia, A.M. Dabas, P. Delville, A. Protat, O. Reitebuch, and C. Werner, 2005: Summer mistral at the exit of the Rhône valley. *Quart. J. Roy. Meteor. Soc.*, **131**, 353-375.

Elgered, G., 1993: Tropospheric radio path delay from ground-based microwave radiometry. In *Atmospheric Remote Sensing by Microwave Radiometry*. Janssen, M.A. (Ed.), John Wiley, pp. 215-258.

Emardson, T.R., and H.J.P. Derks, 1999: On the relation between the wet delay and the integrated precipitable water vapour in the European atmosphere. *Meteorological Applications*, **6**, 1-12.

Elòsegui, P., J.L. Davis, L.P. Gradinarsky, G. Elgered, J.M. Johansson, D.A. Tahmoush, and A. Rius, 1999: Sensing atmospheric structure using small-scale space geodetic networks, *Geophys. Res. Lett.*, **26**, 2445-2448.

- Falvey, M., and J. Beavan, 2002: The impact of GPS precipitable water assimilation on mesoscale model retrievals of orographic rainfall during SALPEX'96. *Mon. Wea. Rev.*, **130**, 2874-2888.
- Flores, A., G. Ruffini, and A. Rius, 2000: 4D tropospheric tomography using GPS wet slant delays. *Ann. Geophys.*, **18**, 223-234.
- Foelsche, U., and G. Kirchengast, 2001: Tropospheric water vapor imaging by combination of ground-based and spaceborne GNSS sounding data. *J. Geophys. Res.*, **106**, 27221-27231.
- Gradinarsky, L., 2002: *Sensing atmospheric water vapor using radio waves*. PhD Thesis, Department of Radio and Space Science, School of Electrical Engineering, Chalmers University of Technology, Gfteborg, Sweden.
- Guénard, V., P. Drobinski, J.-L. Caccia, B. Campistron, and B. Bénéch, 2005: Experimental investigation of the mesoscale dynamics of the Mistral. *Bound.-Layer Meteor.*, **115**, 263-288.
- Haase, J., M. Ge, H. Vedel and E. Calais, 2003: Accuracy and variability of GPS trpospheric delay measurements of water vapor in the western Mediterranean. *J. Appl. Meteor.*, **42**, No 11, 1547-1568.
- Jànsa, A., 1987: Distribution of the mistral: A satellite observation. *Meteor. Atmos. Phys.*, **36**, 201-214.
- Jarlemark, P., J. Johansson, B. Stoew, L. Gradinarsky, and G. Elgered, 2001: Spatial error correlations of GPS atmopsheres as determined from simulations. *Phys. Chem. Earth*, **26 (A6-8)**, 451-456.

- Jiang, Q., Smith, R.B., and Doyle, J.D., 2003: The nature of the mistral: Observations and modeling of two MAP events. *Quart. J. Roy. Meteor. Soc.*, **129**, 857-876.
- Kambezidis, H. D., D., Weidauer, D. Melas, and M. Ulbricht, 1998: Air quality in the Athens basin during sea-breeze and non-sea breeze days using laser-remote-sensing technique. *Atmos. Env.*, **32**, 2173-2182.
- Koo, Y.S., and D.D. Reible, 1995: Flow and transport modeling in the sea breeze. Part II: Flow model application and pollutant transport. *Boun.-Lay. Meteor.*, **75**, 209-234.
- Lemonsu, A., S. Bastin, V. Masson, and P. Drobinski, 2006: Vertical structure of the urban boundary layer over Marseille under sea breeze condition. *Bound.-Layer Meteor.*, in press.
- Leveque, J.-J., and F. Masson, 1999: From ACH tomographic models to absolute velocity models, *Geophys. J. Int.*, **137**, 621-629.
- MacDonald, A. E., Y. Xie, and R. Ware, 2002: Diagnosis of three dimensional water vapor using a GPS network. *Mon. Wea. Rev.*, **130**, 386-397.
- Mayençon, R., 1982: *Météorologie Pratique*. Editions Maritimes et d'Outre-Mer, Paris.
- Niell, A.E., A.J. Coster, F.S. Solheim, V.B. Mendes, P.C. Toor, R.B. Langley, and C.A. Upham, 2001: Comparison of measurements of atmospheric wet delay by radiosonde, water vapor radiometer, GPS, and VLBI. *J. Atmos. Oceanic Technol.*, **18**, 830-850.
- Pettré, P., 1982: On the problem of violent valley winds. *J. Atmos. Sci.*, **39**, 542-554.
- Simpson, J.E., 1994: *Sea breeze and local winds*. Cambridge University Press, U.K., 234 pp.
- Shoji, Y., H. Nakamura, T. Iwabuchi, K. Aonashi, H. Seko, K. Mishima, A. Itagaki, R. Ichikawa,

and R. Ohtani, 2004: Tsukuba GPS Dense net campaign observation: Improvement in GPS analysis of slant path delay by stacking one-way postfit phase residuals. *J. Meteorol. Soc. of Japan*, **82**, 301-314.

Walpersdorf, A., O. Bock, E. Doerflinger, F. Masson, J. Van-Baelen, A. Somieski, and B. Bürki, 2004: Data analysis of a dense GPS network operated during the ESCOMPTE campaign: First results, *Phys. Chem. Earth*, **29**, 201-211.

Weckwerth, T.M., D.B. Parsons, S.E. Koch, J.A. Moore, M.A. Lemone, B.B. Demoz, C. Flamant, B. Geerts, J. Wang, and W.F. Feltz, 2004: An overview of the International H2O Project (IHOP_2002) and some preliminary highlights. *Bull. Amer. Meteorol. Soc.*, **85**, 253-277.

FIGURE CAPTIONS

Figure 1 : Panel a: Map of France with the topography shaded in grey when higher than 500 m ASL. The rectangle displays the region shown in panel b. Panel b: Zoom of the region shown with a rectangle in panel a. The acronyms AIX, LYO, NIM and MRS correspond to the city names Aix-les-Milles, Lyon, Nîmes and Marseille, respectively. The rectangle around MRS displays the limits of the GPS network deployed in the city of Marseille. This network is shown in panel c. The 17 GPS receivers have a mean distance between them of about 5 km and their associated acronyms correspond to district names or building names of the city. Filled contours of topography are indicated with an increment of 100 m. The rectangle in dashed-line indicates the limits of the domain represented in Figure ??.

Figure 2 : Synoptic situation in 12-hourly intervals on 22 June 2001 at 0000 UTC (a) and 1200 UTC (b), 25 June 2001 at 0000 UTC (c) and 1200 UTC (d) and 26 June 2001 at 0000 UTC (e) and 1200 UTC (f) from ECMWF analyses. The mean sea-level pressure and 500-hPa geopotential heights are shown with solid (the contour interval is 2 hPa) and thick dashed (the contour is 50 m) lines, respectively.

Figure 3 : Wind and temperature fields from meteorological surface stations on 22 June 2001 at 0000 UTC (a) and 1200 UTC (b), 25 June 2001 at 0000 UTC (c) and 1200 UTC (d) and 26 June 2001 at 0000 UTC (e) and 1200 UTC (f). The topography mask corresponds to topographical elements higher than 500 m ASL. The arrows indicate the wind direction and their scale indicate the intensity. The isolines indicate the temperature. Contour interval is 3°C from 15 to 36°C. The acronym MRS indicates the location of Marseille.

Figure 4 : Panel a: Time versus height plots of wind speed over the center of Marseille (close to the GPS station named CINQ, see Figure 1) as retrieved from the UHF measurements between June 21 and June 26. Panel b: Same as panel a but for the wind direction. Panel c: Time versus height plot of water vapor density retrieved from GPS tomography between June 21 and June 26 within the Marseille city center at 5.375°E longitude and 43.325°N latitude. The black ticks indicate the times of the assimilated radiosondes. Panel d: Time series of the integrated water vapor (IWV) from GPS between June 21 and June 26 at Vallon d'Ol (VALL, northern suburbs of Marseille) and CINQ (Marseille city center). The labels (i), (ii), (iii), (iv) and (v) indicates the origin of the IWV variability: (i) sea breeze advecting inland marine moist air; (ii) Mistral advecting continental dry air from the northwest; (iii) land breeze advecting offshore the moist air advected inland by the preceding sea breeze and having experienced cooling and condensation; (iv) easterly synoptic flow; (v) combination of sea breeze with prevailing continental southeasterly flow.

Figure ?? : IWV spatial variations from the ESCOMPTE GPS network on 22 June 2001 at 0600 (a), 1200 (b) and 1800 (c) UTC, on 25 June at 0600 (d), 1200 (e) and 1800 (f) UTC, and on 26 June at 0600 (g), 1200 (h) and 1800 (i) UTC.

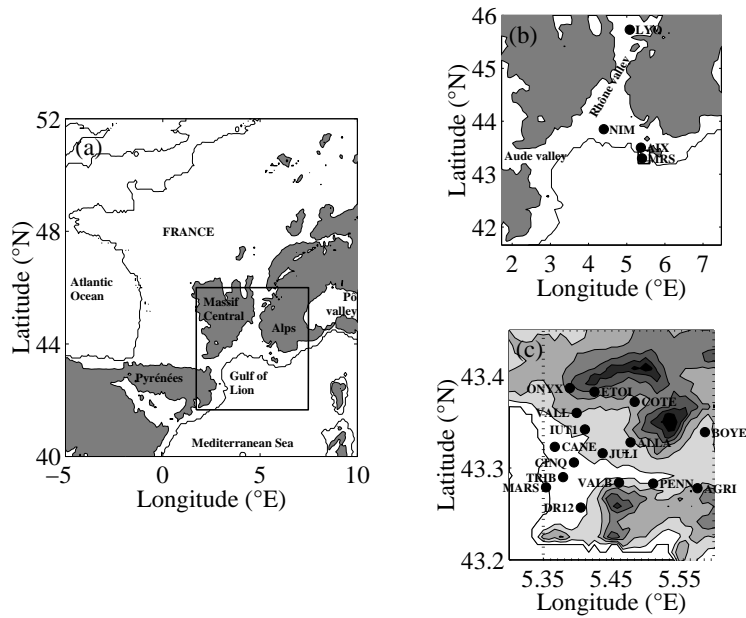


Figure 1: Panel a: Map of France with the topography shaded in grey when higher than 500 m above sea level. The rectangle displays the region shown in panel b. Panel b: Zoom of the region shown with a rectangle in panel a. The acronyms AIX, LYO, NIM and MRS correspond to the city names Aix-les-Milles, Lyon, Nîmes and Marseille, respectively. The rectangle around MRS displays the limits of the GPS network deployed in the city of Marseille. This network is shown in panel c. The 17 GPS receivers have a mean distance between them of about 5 km and their associated acronyms correspond to district names or building names of the city. Filled contours of topography are indicated with an increment of 100 m. The rectangle in dashed-line indicates the limits of the domain represented in Figure ??.

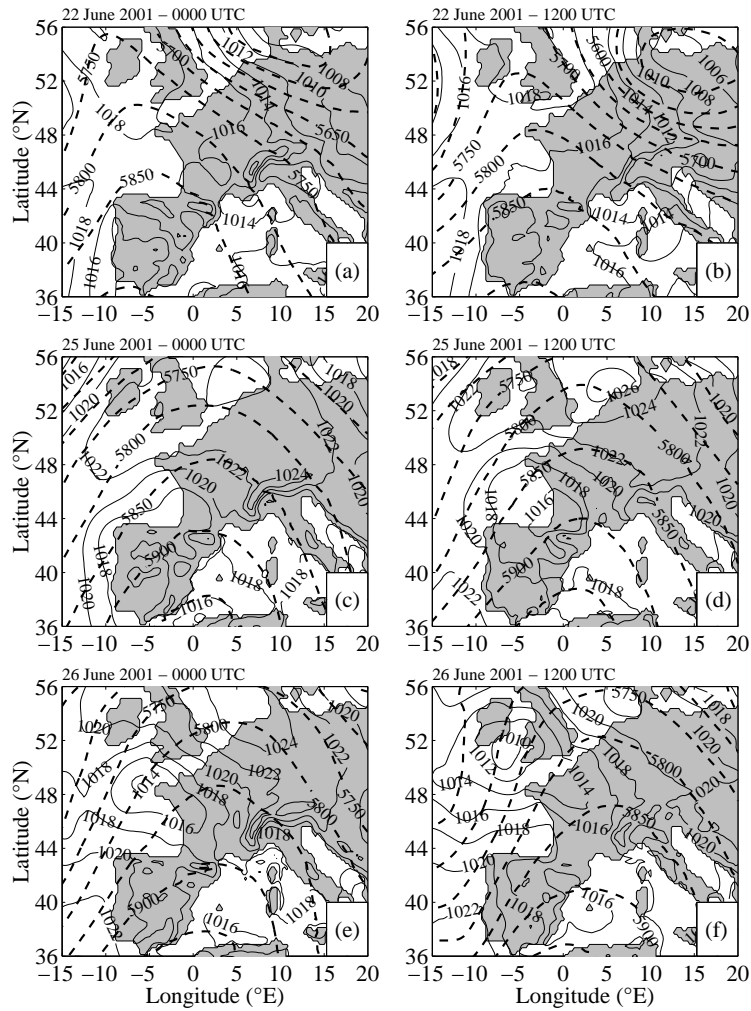


Figure 2: Synoptic situation in 12-hourly intervals on 22 June 2001 at 0000 UTC (a) and 1200 UTC (b), 25 June 2001 at 0000 UTC (c) and 1200 UTC (d) and 26 June 2001 at 0000 UTC (e) and 1200 UTC (f) from ECMWF analyses. The mean sea-level pressure and 500-hPa geopotential heights are shown with solid (the contour interval is 2 hPa) and thick dashed (the contour is 50 m) lines, respectively.

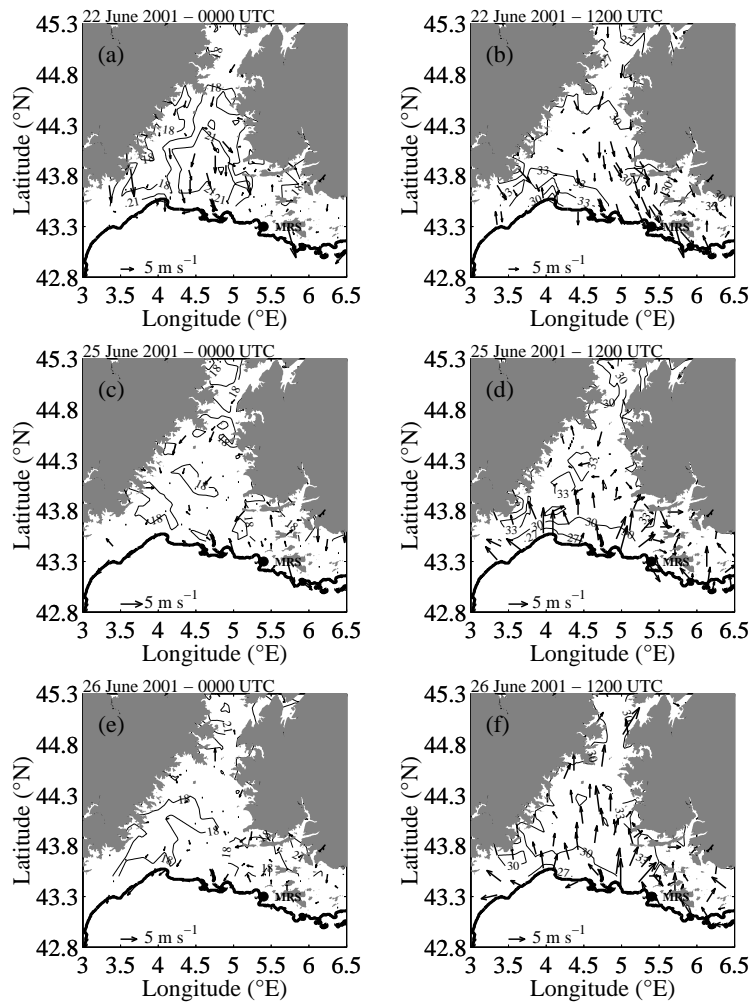


Figure 3: Wind and temperature fields from meteorological surface stations on 22 June 2001 at 0000 UTC (a) and 1200 UTC (b), 25 June 2001 at 0000 UTC (c) and 1200 UTC (d) and 26 June 2001 at 0000 UTC (e) and 1200 UTC (f). The topography mask corresponds to topographical elements higher than 500 m ASL. The arrows indicate the wind direction and their scale indicate the intensity. The isolines indicate the temperature. Contour interval is 3°C from 15°C to 36°C . The acronym MRS indicates the location of Marseille.

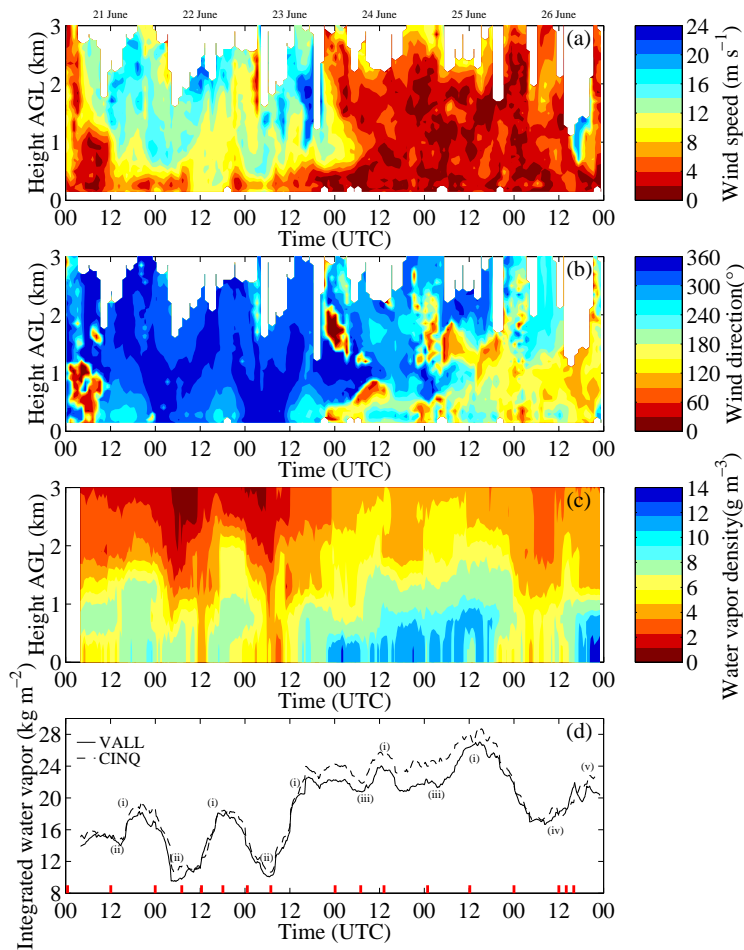


Figure 4: Panel a: Time versus height plots of wind speed over the center of Marseille (close to the GPS station named CINQ, see Figure 1) as retrieved from the UHF measurements between June 21 and June 26. Panel b: Same as panel a but for the wind direction. Panel c: Time versus height plot of water vapor density retrieved from GPS tomography between June 21 and June 26 within the Marseille city center at 5.375°E longitude and 43.325°N latitude. The black ticks indicate the times of the assimilated radiosondes. Panel d: Time series of the integrated water vapor (IWV) from GPS between June 21 and June 26 at Vallon d'Ol (VALL, northern suburbs of Marseille) and CINQ (Marseille city center). The labels (i), (ii), (iii), (iv) and (v) indicates the origin of the IWV variability: (i) sea breeze advecting inland marine moist air; (ii) Mistral advecting continental dry air from the northwest; (iii) land breeze advecting offshore the moist air advected inland by the preceding sea breeze and having experienced cooling and condensation; (iv) easterly synoptic flow; (v) combination of sea breeze with prevailing continental southeasterly flow.